FOUNDATIONS
ADVANCES

ISSN: 2053-2733
journals.iucr.org/a

Computer simulations of X-ray six-beam diffraction in a perfect silicon crystal. I

V. G. Kohn and D. R. Khikhlukha

Acta Cryst. (2016). A**72**, 349–356

Acta Cryst A FOUNDATIONS ADVANCES

ISSN 2053-2733

Computer simulations of X-ray six-beam diffraction in a perfect silicon crystal. I

V. G. Kohn[a]* and D. R. Khikhlukha[b]

[a]National Research Centre 'Kurchatov Institute', 123182 Moscow, Russian Federation, and [b]Extreme Light Infrastructure, Institute of Physics ASCR, 18221 Praha 8, Czech Republic. *Correspondence e-mail: kohnvict@yandex.ru

Received 18 November 2015
Accepted 1 February 2016

Edited by L. D. Marks, Northwestern University, USA

Keywords: X-ray diffraction; silicon crystal; six-beam diffraction; section topography; computer simulations.

This paper reports computer simulations of the transmitted-beam intensity distribution for the case of six-beam (000, 220, 242, 044, −224, −202) diffraction of X-rays in a perfect silicon crystal of thickness 1 mm. Both the plane-wave angular dependence and the six-beam section topographs, which are usually obtained in experiments with a restricted beam (two-dimensional slit), are calculated. The angular dependence is calculated in accordance with Ewald's theory. The section topographs are calculated from the angular dependence by means of the fast Fourier transformation procedure. This approach allows one to consider, for the first time, the transformation of the topograph's structure due to the two-dimensional slit sizes and the distance between the slit and the detector. The results are in good agreement with the results of other works and with the experimental data. This method of calculation does not require a supercomputer and it was performed on a standard laptop. A detailed explanation of the main features of the diffraction patterns at different distances between the slit and the detector is presented.

1. Introduction

The phenomenon of six-beam (000, 220, 242, 044, −224, −202) X-ray diffraction in perfect crystals of silicon and germanium in transmission experiments became interesting for physicists after the publication of the work by Joko & Fukuhara (1967). They presented the analytical formulae for all eigenvectors of the plane-wave scattering matrix at the central point on the two-dimensional area of angular deviations in which all Bragg conditions are met accurately. These eigenvectors were used by the authors to show that the absorption coefficient for a part of the radiation is very small compared to the two-beam case.

A detailed study of this question was given by Afanas'ev & Kohn (1977*a*). They carefully calculated the dipole and quadrupole contributions to the photoelectric absorption under the conditions of the two-dimensional standing wave arising due to the six-beam diffraction. Later on Kohn (1987*a*,*b*) showed a way to take into account the contribution of the Compton scattering to the wave attenuation for the eigenvectors with a low absorption coefficient.

It was shown from the calculation of the intensity angular dependence for the transmitted plane wave (Kon, 1976*a*,*b*) that the maximum intensity does not correspond to the central point, where the parameters of deviation from the Bragg conditions equal zero, but is shifted to the left. At the same time, the minimum absorption coefficient corresponds to the central point. This effect of asymmetry is absent in the two-beam case. Such asymmetry was shown to be associated with the presence of a large number of eigenvectors with close values of the dispersion corrections.

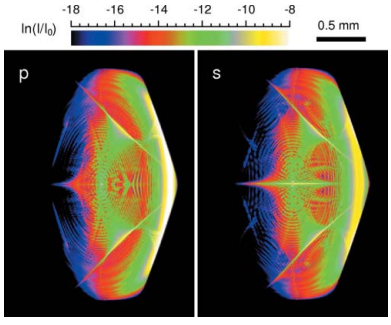

Since it is very difficult to make a plane wave in a laboratory experiment, Huang *et al.* (1973) have proposed a simple transmission scheme for experimental study of six-beam diffraction. In this scheme the radiation from the source of size 100×100 μm was incident on the crystal, located at a distance of 6 cm, whereas a photographic plate was located at a relatively large distance (2 m) from the crystal.

The angular divergence of the incident beam was large, which allows one to fix on a photographic plate the intersecting stripes of two-beam anomalous transmission separately for $K_{\alpha 1}$, $K_{\alpha 2}$ and K_{β} lines in the spectrum of the characteristic radiation of a copper anode with the photon energy of $E = 8$ keV. However, they failed to observe an enhancement of the brightness at the point of intersection.

Later, this scheme was modified by Kshevetskii & Mikhailyuk (1976*a*,*b*). They increased the distance between the source and the crystal (more than 2 m) and put a photographic plate directly behind the crystal. However, the main difference was the use of a microfocus X-ray tube with the source linear dimensions of a few microns. The authors found an increased intensity in the area of two-beam stripe intersection, but this effect was apparent only for the intermediate thickness of the crystal and it disappeared for thicker crystals.

In the work by Kohn & Toneyan (1986) the theory of the multi-beam diffraction of X-ray spherical waves was presented. It was shown by means of approximate computer calculations that the intensity distribution on the photographic plate in the experimental scheme described above strongly depends on the distance. It was also shown that the observed intensity increase is not associated with absorption, but with the effect of diffraction focusing of the spherical wave (Afanas'ev & Kon, 1977*b*,*c*; Kon, 1977*a*,*b*).

It should be noted that synchrotron radiation for the experiment of such a scheme was used by Chang (1982*a*,*b*). The source was located at a distance of 32 m from the crystal and the photographic plate was located at a distance of 20 cm. For $E = 8$ keV and a silicon crystal of thickness 3 mm the author observed an image of the output window of synchrotron radiation without the two-beam stripes.

In the papers of Huang *et al.* (1973) and Chang (1982*b*) the results of calculations of the intensity angular dependence for the transmitted plane wave were presented. However they cannot be valid though because the distribution was symmetric in two directions. This property does not correspond to reality. The presence of asymmetry in the intensity of the transmitted wave follows from the experiments of Umeno (1970, 1972, 1976*a*,*b*).

A new approach in the study of six-beam diffraction in a transmission case was used in the work of Okitsu (2003) and Okitsu *et al.* (2003). The authors rejected a calculation of the angular dependence of the plane-wave amplitudes and solved the system of differential equations directly. This system is a generalization of the known two-beam Takagi equations (Takagi, 1962) in the six-beam case. In this approach, one begins with a point source on the entrance surface of the crystal and ends on the output surface, *i.e.* the solution is carried out only in the volume of the crystal.

In the case of two-beam diffraction, this method is usually used to study defects in the crystal. In reality, a point source is formed by a narrow slit in front of the crystal. If the thickness of the crystal is much larger than the size of the slit, then distortion of the central part of the diffraction pattern due to the slit is relatively small. This method is called section topography, because it refers to the intensity distribution of transmitted and reflected beams in real space rather than in angular space and in a restricted domain.

In the works of Heyroth *et al.* (1999) and Kohn & Smirnova (2015) the effect of multi-beam diffraction on the two-beam section topographs of the reflected beam, which consists of stripes of equal intensity along the slit, was investigated. In this case, the incident beam represents a mixture of waves from different sources in different directions. In the direction across the slit the effective source is the slit itself mounted in front of the crystal. In the direction along the slit one deals with the real source located relatively far from the crystal.

To obtain the section topographs of six-beam diffraction the slit should be rectangular to limit the beam in two dimensions. To reduce the effect of a large two-dimensional slit (1×1 mm) on the result of the experiment in the works of Okitsu (2003) and Okitsu *et al.* (2003) the authors had to use hard radiation of 18.5 keV and a thick crystal (thickness of 9.9 mm). Moreover, they examined the case with doubled Miller indices, *i.e.* (000, 440, 484, 088, −448, −404), to maximize the size of the image compared to the size of the slit.

As a result, they obtained a very good agreement between the experimental and computed six-beam section topographs, even without taking into consideration the size of the slit in the calculations. In subsequent works by Okitsu *et al.* (2006, 2011), the authors used a slit with a smaller size, 100×100 μm, and considered a sample shape different from a plate, which is commonly used in the study of the diffraction of plane waves.

In this paper we present the results of computer simulations of X-ray six-beam section topographs for the transmitted beam with high accuracy, *i.e.* taking into account the interference between various eigenvectors of the diffraction problem. The calculation is performed by means of the fast Fourier transformation (FFT) procedure applied on two-dimensional functions of angular dependence of the wavefield amplitudes for different polarizations. This approach allows us to investigate the impact of the slit size and distances along the beam on the structure of a section topograph.

2. Formulation of the problem

Let us consider a silicon crystal having a platelet shape with a surface normal to the direction 1−11 of the cubic crystal lattice. Let $\mathbf{n}_0$ be a unit vector along this direction. There are six points in the reciprocal lattice with the Miller indices (000, 220, 242, 044, −224, −202) at the plane normal to $\mathbf{n}_0$, which form a regular hexagon (Fig. 1). Let the wavevector of the incident plane wave $\mathbf{k}_0$ form the angle θ_0 with the vector $\mathbf{n}_0$, and $\sin\theta_0 = 8^{1/2}\lambda/a$, where λ is the wavelength of radiation, a is the silicon crystal lattice parameter. If the end of the $\mathbf{k}_0$ vector coincides with the origin of the reciprocal lattice (000),

then for all the above-mentioned reciprocal-lattice vectors $\mathbf{h}_m$, $m = 0, \ldots, 5$, the Bragg condition $|\mathbf{k}_m|^2 = |\mathbf{k}_0|^2$ is met, where $\mathbf{k}_m = \mathbf{k}_0 + \mathbf{h}_m$.

We choose the $\mathbf{k}_0$ direction as the Z axis of the Cartesian coordinate system. We assume that the source of X-ray synchrotron radiation is located on this axis, the distance between the source and the crystal is large, and the source angular divergence is small. We assume as well that a two-dimensional slit of rectangular shape is mounted in front of the crystal. Then for a wave incident on the slit we can use a paraxial approximation and represent it by the parabolic wave.

In front of the slit the electric field vector of the radiation can be written in the form

$$\mathbf{E}_0(x, y, 0) = C\mathbf{e}_{0i} \exp(iKz_0) P_2(x, y, z_0). \quad (1)$$

Here C is the normalization factor, which does not influence the relative intensity, $\mathbf{e}_{0i}$ is the unit vector of polarization, $K = 2\pi/\lambda$ is the wavenumber, z_0 is the distance between the source and the slit, $P_2(x, y, z)$ is the two-dimensional Fresnel propagator, namely,

$$P_2(x, y, z) = P(x, z)P(y, z), \quad (2)$$

where

$$P(x, z) = (i\lambda z)^{-1/2} \exp(i\pi x^2/\lambda z). \quad (3)$$

The characteristic radiation of X-ray tubes is not polarized. Therefore, in this case the final results should be averaged over the polarization states. As for synchrotron radiation, it is polarized inside the plane of electron orbit, *i.e.* a horizontal plane.

The two-dimensional slit in front of the crystal has two functions. Firstly, it limits the size of the beam which is important to highlight a section of a crystal without defects or with a given defect. Secondly, it forms the angular divergence of the radiation, if the size of the slit is less than the transverse coherence length of the radiation.

It is important to understand that the conditions in a laboratory experiment and in experiments on the synchrotron-radiation source are significantly different. The transverse coherence length $L_{tc} = \lambda/2\alpha$, where $\alpha = w_s/z_0$ is the angular size of the source at the distance from the source to the slit (Kohn *et al.*, 2000, 2001). In the first case, the angular size of the source typically is very large, and the transverse coherence length is much smaller than the slit size. The slit plays the role of a secondary incoherent source with a large radiation divergence.

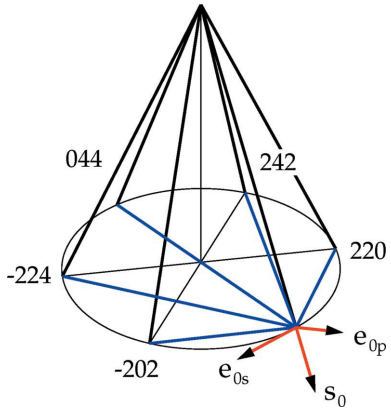

Figure 1
The geometry of six-beam diffraction. The directions of the beams, the directions of the two-beam stripes for each reflection, and the polarization vectors for the incident wave are shown.

For third-generation synchrotron-radiation sources, where $\alpha = 1$ μrad and $\lambda = 0.15$ nm, we have $L_{tc} = 75$ μm. Now the slit has a size generally comparable to or less than L_{tc}. Accordingly, the incident wave is modified specifically due to diffraction at the slit. On the other hand, the diameter of the first Fresnel zone of the propagator $P(x, z)$ at $\lambda = 0.15$ nm and $z_0 = 50$ m is equal to $D = 2(\lambda z_0)^{1/2} = 170$ μm. Thus, in the region of the slit the incident radiation can be considered as a plane wave.

As a result, if the wave amplitude is normalized by the value in front of the slit, then for the vector $\mathbf{E}_0$ just after the slit we have

$$\mathbf{E}_0(x, y, 1) = \mathbf{e}_{0i} \exp(iKz_0)\, T(x, y), \quad (4)$$

where

$$T(x, y) = \theta(x_0 - |x|)\, \theta(y_0 - |y|). \quad (5)$$

Here $\theta(x)$ is the Heaviside function which is equal to unity for $x > 0$ and to zero for $x < 0$, and the values x_0, y_0 are equal to half sizes of the slit along the axes x and y correspondingly. Let the distance between the slit and the crystal be z_1. The wavefunction of radiation in front of the crystal is calculated by means of the Kirchhoff formula and is equal to a convolution of the function (4) with the Fresnel propagator (2) for the distance z_1. Below, for the sake of simplicity, we omit the phase factor $\exp(iKz_0)$, connected with the motion along the z axis, because it does not influence the registered relative intensity.

As a result, we obtain for the vector $\mathbf{E}_0$ in front of the crystal

$$\mathbf{E}_0(x, y, 2) = \mathbf{e}_{0i}\psi_{2i}(x, y), \quad (6)$$

where

$$\psi_{2i}(x, y) = P_2(x - x_1, y - y_1, z_1) * T(x_1, y_1). \quad (7)$$

Here and below, the symbol $*$ means integrating over the twice-repeated variables in function arguments. Diffraction of the X-ray wave in the crystal leads to a transmitted wave arising and five diffracted waves moving in various directions. In this paper we are concerned with the transformation of the transmitted wave, which does not change its direction. It is convenient for experiments with synchrotron radiation.

Since the perfect crystal structure is homogeneous along the surface, the result of diffraction can be written as a convolution of the function (7) with the function called the propagator of the crystal $P_C^{vi}(x, y, t)$, which depends on the crystal thickness t and indices of polarization for the input i and output v radiation.

As a result, for the vector $\mathbf{E}_0$ just behind the crystal we have

$$\mathbf{E}_0(x, y, 3) = \sum_v \mathbf{e}_{0v}\psi_{3v}(x, y), \tag{8}$$

where

$$\psi_{3v}(x, y) = P_C^{vi}(x - x_1, y - y_1, t) * \psi_{2i}(x_1, y_1). \tag{9}$$

It should be noted that the crystal forms an angle θ_0 with the Z axis; therefore the wavefunctions (7) and (9) are not defined at input and output surfaces of the crystal. They are defined in the planes normal to the Z axis (Fig. 2). However, one can use the crystal propagator for the radiation transfer from the input surface to the output surface because the additional phase factor along the z axis does not depend on the coordinates x and y.

If a detector is located at some distance from the crystal z_2, then the vector of the electric field at the detector is determined by the convolution of the Fresnel propagator with the field of equation (8), namely,

$$\mathbf{E}_0(x, y, 4) = \sum_v \mathbf{e}_{0v}\psi_{4v}(x, y), \tag{10}$$

where

$$\psi_{4v}(x, y) = P_2(x - x_1, y - y_1, z_2) * \psi_{3v}(x, y). \tag{11}$$

Substituting the formula (7) into (9) and then (9) into (11), we obtain a convolution of four functions. Now we apply a well known rule that the multipliers in the convolution can be interchanged, and that the convolution of two Fresnel propagators is equal to the Fresnel propagator at the total distance. As a result, we finally have

$$\psi_{4v}(x, y) = P_2(x - x_2, y - y_2, z_t) * P_C^{vi}(x_2 - x_1, y_2 - y_1, t) * T(x_1, y_1) \tag{12}$$

where $z_t = z_1 + z_2$. It follows from this expression that the wavefunction does not depend on the location of the crystal inside the path of the beam from the slit to the detector. Only the total distance z_t is important.

For the calculation of the wavefunction $\psi_{4v}(x, y)$ we use the Fourier transformation in the form

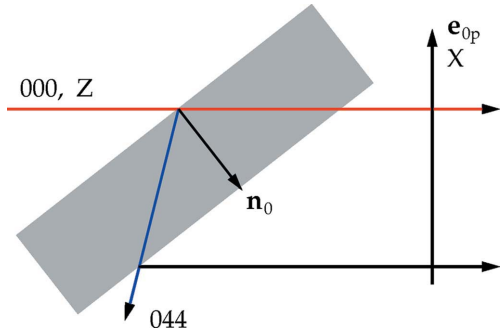

Figure 2
Geometry of the beam widening in the plane of two-beam diffraction for the reflection 044.

$$\psi_{4v}(x, y) = \int \frac{dqdp}{(2\pi)^2}\exp(iqx + ipy) \times P_{Cf}^{vi}(q, p, t)\, P_{2f}(q, p, z_t)\, T_f(q, p). \tag{13}$$

This integral is calculated by means of the FFT procedure and the multipliers of the integrand are calculated directly. So we have

$$P_{2f}(q, p, z) = \exp\left[-i\frac{\lambda z}{4\pi}(q^2 + p^2)\right], \tag{14}$$

$$T_f(q, p) = 4x_0y_0\,\mathrm{sinc}\,(qx_0)\mathrm{sinc}\,(py_0), \tag{15}$$

where

$$\mathrm{sinc}\,(x) = \frac{\sin(x)}{x}. \tag{16}$$

The function $P_{Cf}^{vi}(q, p, t)$ describes the angular dependence of the plane-wave transmission through the crystal under conditions of multiple (six-beam) diffraction, which is calculated previously, for example, by Kon (1976*a*,*b*). Below we describe briefly the method of calculation. If the plane monochromatic wave is incident on the crystal with the wavevector $\mathbf{k}_0' = \mathbf{k}_0 + \mathbf{u}$, where $\mathbf{u}$ is the two-dimensional vector in the plane (x, y) with coordinates q and p, then it experiences refraction inside the crystal and the wavevector becomes equal to $\mathbf{k}_0' + \varepsilon\mathbf{n}_0/2$. Diffraction of the plane wave incident on atomic planes causes the appearance of additional plane waves with the wavevectors $\mathbf{k}_m' + \varepsilon\mathbf{n}_0/2$, where $\mathbf{k}_m' = \mathbf{k}_0' + \mathbf{h}_m$, $\mathbf{h}_m$ are the vectors of the reciprocal lattice of the considered multi-beam configuration, which satisfy the Bragg condition $|\mathbf{k}_m'|^2 = |\mathbf{k}_0'|^2$ at $\mathbf{u} = 0$.

The vector amplitude of the electric field of the plane wave with the index m has two components in the plane perpendicular to $\mathbf{k}_m$. We enumerate these components by the index $v = p, s$. Accordingly, for each plane wave we have the three unit vectors $\mathbf{s}_m$, $\mathbf{e}_{mp}$ and $\mathbf{e}_{ms}$. For $m = 0$ the three vectors are shown in Fig. 1. It is possible to choose the unit vectors of the polarization arbitrarily, but it is convenient to use symmetry properties of the multi-beam pyramid, as was first proposed by Joko & Fukuhara (1967). In this case, all the vectors $\mathbf{e}_{ms}$ lie in the plane of reciprocal-lattice vectors, and $\mathbf{e}_{mp} = (\mathbf{e}_{ms} \times \mathbf{s}_m)$.

We denote the scalar components of the electric field vector by $\gamma_m^{-1/2}E_{mv}$, where the multiplier $\gamma_m = (\mathbf{k}_m\mathbf{n}_0)$ is introduced for convenience. Maxwell's equation for the total electric field in the crystal is divided into a system of equations for each component E_{mv}.

This system can be rewritten in the form of the eigenvalue problem:

$$\sum_{nv'} G_{mn}^{vv'}E_{nv'} = \varepsilon E_{mv} \tag{17}$$

for the scattering matrix G, which has the following form in the dipole approximation:

$$G_{mn}^{vv'} = -\frac{K\alpha_m}{\gamma_m}\delta_{mn}\delta_{vv'} + \frac{K\chi_{m-n}}{(\gamma_m\gamma_n)^{1/2}}(\mathbf{e}_{mv}\mathbf{e}_{nv'}) \tag{18}$$

where the parameter $\alpha_m = (|\mathbf{k}_m'|^2 - |\mathbf{k}_0'|^2)/K^2$ depends on the angles $\theta = q/K$ and $\varphi = p/K$, and the diffraction parameters

χ_m are the complex values which describe the amplitudes of kinematical scattering by unit volume of the crystal. In this work they are calculated by means of the program described by Kohn (2006*a*,*b*).

The matrix G describes both the elastic scattering (the real part of the matrix G') and the absorption (the imaginary part of the matrix G''). In our case the matrix elements of G'' are much less than the matrix elements of G'. This allows us to take them into account by means of perturbation theory.

Now the eigenvalue problem of equation (17) is solved only for the real matrix G', which speeds up the calculations. As a result, we obtain $2N$ eigenvectors, where $N = 6$ is the number of beams in the multi-beam configuration. The absorption coefficients are calculated later by means of the formula

$$\mu_j = \varepsilon_j'' = \sum_{m\nu,n\nu'} E_{m\nu}^{(j)} (G'')_{mn}^{\nu\nu'} E_{n\nu'}^{(j)} \tag{19}$$

where an index j enumerates the eigenvalues.

We note that for the real part of the matrix G' it is sufficient to consider only the dipole part of the scattering matrix, since the Thomson scattering on the electron density of atoms gives the main contribution, which is a pure dipole process. However, the imaginary part G'' is determined only by the processes of photoelectric absorption and Compton scattering.

Therefore, under conditions of a sharp weakening of the dipole part of the photoelectric absorption the quadrupolar part can play a role, as well as Compton scattering, which under normal conditions are small and can be neglected. For this reason, the formula (18) inaccurately describes the imaginary part of the scattering matrix G''. As shown by Afanas'ev & Kohn (1977) and Kohn (1987*a*,*b*), to calculate the absorption coefficients one needs to use the matrix in the following form:

$$\begin{aligned}(G'')_{mn}^{\nu\nu'} = {} & \frac{K\chi''_{m-n}}{(\gamma_m\gamma_n)^{1/2}}\left\{(1-Q)(\mathbf{e}_{m\nu}\mathbf{e}_{n\nu'})\right. \\ & \left. +Q[(\mathbf{e}_{m\nu}\mathbf{e}_{n\nu'})(\mathbf{s}_m\mathbf{s}_n)+(\mathbf{e}_{m\nu}\mathbf{s}_n)(\mathbf{e}_{n\nu'}\mathbf{s}_m)]\right\} \\ & +\frac{C_{CS}K\chi'_{m-n}}{(\gamma_m\gamma_n)^{1/2}}(\mathbf{e}_{m\nu}\mathbf{e}_{n\nu'})\end{aligned} \tag{20}$$

where χ''_{m-n} has to be calculated from the experimental value of the photoelectric absorption coefficient, $Q = \sigma_{\rm Q}/(\sigma_{\rm D}+\sigma_{\rm Q})$, $\sigma_{\rm D,Q}$ are cross sections of the dipole and quadrupolar contributions to the photoelectric absorption, $C_{CS} = 4\pi r_0/3\lambda$, $r_0 = e^2/mc^2$ is the classic electron radius. The values of Q were calculated in the work of Hildebrandt *et al.* (1975).

Each eigenvector comes in the full field with the weight $\lambda_j(\varphi)$, which is determined from the boundary conditions and depends on the state of polarization of the incident wave. The boundary conditions are applied to the input surface of the crystal. If the incident wave is polarized and the polarization vector $\mathbf{e}_{0i}$ makes an angle φ with the vector $\mathbf{e}_{0p}$ then they look like

$$\sum_j \lambda_j(\varphi) E_{m\nu}^{(j)} = \gamma_0^{1/2}\delta_{m0}C_\nu(\varphi). \tag{21}$$

Here we assume that the incident wave amplitude is equal to unity, $C_p = \cos\varphi$, $C_s = \sin\varphi$.

Taking into account the orthonormality of the eigenvectors, the system of equation (21) is easily solved, and results in

$$\lambda_j(\varphi) = \gamma_0^{1/2}[E_{0p}^{(j)}C_p + E_{0s}^{(j)}C_s]. \tag{22}$$

Finally, the transmission amplitude of the polarized plane wave through the crystal is equal to

$$P_{Cf}^{vi}(q,p,t) = \gamma_0^{-1/2}\sum_j \lambda_j(\varphi)E_{0\nu}^{(j)}\exp(i\varepsilon_j t/2). \tag{23}$$

In this work we consider two polarization states of the incident wave for which $\varphi = 0$ and $\pi/2$, *i.e.* the vector $\mathbf{e}_{0i}$ is equal to either $\mathbf{e}_{0p}$ or $\mathbf{e}_{0s}$.

3. Results and discussion

In this paper we present the results of computer simulations for the angular dependence of the transmitted-beam intensity as well as for the section topographs in the case of crystal thickness $t = 1$ mm and for the photon energy of $E = 8$ keV, which is close to the Cu K_α line in the spectrum of the X-ray tube. We consider the symmetrical case where all the parameters $\gamma_m = \cos\theta_0 = 0.59$, and the angle $\theta_0 = 53.8^\circ$ is equal to the Bragg angle for the 044 reflection (Fig. 2). In this case, a decrease in intensity due to passage of the plane wave through a crystal is determined by the factor $\exp(-\mu_0 t/\gamma_0) = 3\times10^{-11}$, and therefore the crystal absorbs the radiation completely.

It is known that in the two-beam case of diffraction the absorption coefficient for the path directed along the incident beam $\mu = K(\chi_0'' - \chi_h'')/\gamma_0 = 0.75\ {\rm mm}^{-1}$ for the sigma polarization when the electric field vector is normal to the scattering plane. Accordingly, the decrease in intensity is determined by the factor $\exp(-\mu t) = 0.47$.

We note that the polarization states, considered in this paper, do not coincide with the sigma polarization for the two-beam reflection of type 220. Therefore a decrease in intensity on the two-beam stripes (see Fig. 3) is greater than the value estimated above, and for p polarization the two-beam 220 stripes are more clearly visible, because the vector $\mathbf{e}_{0p}$ has a direction which makes a smaller angle with the direction of sigma polarization for the 220 two-beam case.

Thus, under these parameters the effect of enhancement of anomalous transmission in the case of multi-beam diffraction can be seen, though not in a pronounced form. On the other hand, such thickness of the crystal allows us to study the interference between the various eigenvectors, having a relatively small absorption coefficient under conditions of multi-beam diffraction. As it is known, such interference is absent in the two-beam case.

Since the full amplitude of the radiation field oscillates with small periods on the map of the angular dependence as a result of the interference, the calculation has to be carried out with high resolution. In this work the calculation was performed on a grid with the number of points $n_1 = 4096$ for the angle θ and $n_2 = 2048$ for the angle φ with a constant step $\Delta = 0.04$ μrad.

The angles θ and φ are measured in the directions of the polarization vectors $\mathbf{e}_{0p}$ and $\mathbf{e}_{0s}$, respectively. The computed angular area size is 163.84 × 81.92 μrad.

Fig. 3 shows the central part of the calculated angular area with a size of 81.92 × 40.96 μrad, which contains the entire multi-beam region. In the rest of the computational domain there are only two-beam tails, strongly deformed by multi-beam scattering, as described in the work of Kohn & Smirnova (2015). In order to better represent the intensity variation on different scales, the image shows a logarithm of the intensity normalized to the value of the incident wave. Both axes θ (horizontally) and φ (vertically) have the same units which are shown above the picture. The two-beam stripes are normal to the reciprocal-lattice vectors shown in Fig. 1 by blue lines.

The intensity was calculated as a sum of the square modules of the function (23) for the two values of the index v. As it follows from the calculations, the effect of anomalous transmission enhancement depends on the polarization of the incident radiation, and for the p polarization it is more pronounced than for the s polarization. This takes place for both the two-beam 220 stripes and the six-beam region of angles. The lack of the two-beam stripe for the 044 reflex for p polarization is related to the fact that this polarization accurately meets the pi polarization, as is determined in the two-beam case, and for this polarization the decrease in the absorption coefficient is small, namely $\mu = K(\chi_0'' + \chi_h'' \cos 2\theta_B)/\gamma_0 = 17.8\ \mathrm{mm}^{-1}$.

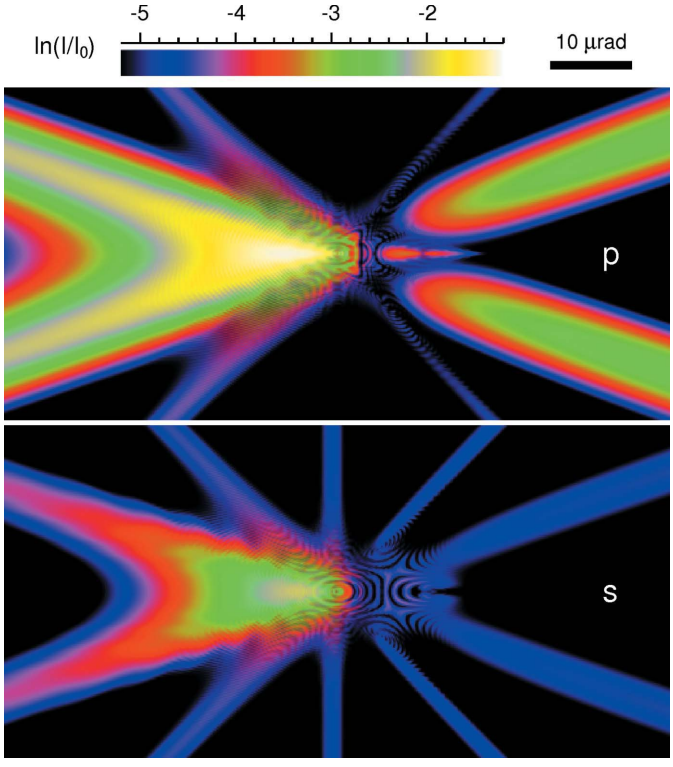

Figure 3
The angular dependence of the logarithm of the transmitted-beam intensity for two polarization states of the incident wave, p (top) and s (bottom). Both axes θ (horizontally) and φ (vertically) have the same units which are shown above the picture.

On the other hand, for s polarization $\mu = K(\chi_0'' - \chi_h'')/\gamma_0 = 2.9\ \mathrm{mm}^{-1}$. Therefore, on the s map this stripe is visible, although in a very attenuated form. Additional weakening is due to the fact that only 1/4 part of the intensity of the incident beam abnormally passes through the crystal. It is easy to verify, by taking the sum of p and s maps, that our result is in general qualitatively consistent with the result presented by Kon (1976*a*,*b*) although it is performed for the other set of parameters.

Calculation of the section topographs was performed as a sum of the square moduli of the function (13) for the two values of the index v. The two-dimensional slit sizes $2x_0$ and $2y_0$ were taken such that the graph of the function $T_f(q, p)$ has the first zero value at the boundaries of the computational domain. Outside the computational domain, this function has small values and oscillates, and, therefore, two-beam tails do not contribute to the topograph. Since the computational domain has different dimensions in the x and y axes, the two-dimensional slit sizes were different too, namely $2x_0$ = 1.892 μm and $2y_0 = 3.784$ μm. In a real experiment, the sizes of the two-dimensional slit can be much larger. Then the two-beam tails are cut off at a smaller distance from the centre of the multi-beam region. But these dimensions can be implemented.

The calculation was performed using the FFT method. In this method the number of points of the computational grid in direct space remains unchanged, but the steps of the grid are determined by the formulas $\Delta_x = 2\pi/(n_1 K \Delta)$ and $\Delta_y = \Delta_x n_1/n_2$. Therefore, the step on the x axis was two times less than the step along the y axis. To make the picture with the same steps, each pair of columns was replaced by one column with a value equal to a half sum of the values in the pair. The resulting picture is square with the number of points 2048 × 2048 and the step $\Delta_y = 1.892$ μm. This value is equal to the horizontal size of the slit and is just two times less than the vertical size. So the picture resolution is commensurate with the size of the slit, and the slit is not visible on the topograph.

The linear size of the computational domain is equal to 3.874 mm for both axes. Fig. 4 shows the simulation results for the distance $z_t = 1$ cm. The horizontal axis in the figure corresponds to the x coordinate shown in Fig. 2. Both axes have the same units which are shown above the picture. The picture shows the part of the computational domain containing an image of the crystal. The two-beam stripes are clearly visible. They correspond to the blue lines in Fig. 1. The stripes for the reflections of type 220 are thicker due to multiple scattering in other reflexes. The stripe corresponding to the 044 reflection is absent on the picture for p polarization.

Six-beam diffraction interference fringes have the shape of ellipses with greater intensity in the areas between the centre of the topograph and the two-beam stripes for the reflections of type 242. On these stripes the intensity maximum is in the middle of them, which can be easily explained by the fact that in the case of two-beam diffraction the energy flow of the slightly absorbed part of the radiation is confined between the directions of incident and diffracted waves.

On the other hand, two-beam stripes of the 220 type interact so strongly that the area between them also remains bright and looks like an arc, which was first observed by Umeno (1970). This area corresponds to the bright area in the left part of Fig. 3. The method of the stationary phase (Kohn & Toneyan, 1986) allows one to determine the direction of the rays corresponding to the points of the angular dependence of the plane-wave diffraction. Using this method it is possible to show that this is just so, and this is due to the structure of the dispersion surface, which can be built from the function $\varepsilon'(\theta, \varphi)$.

The interference fringes contain fragments which look the same for both polarizations, but there are also fragments which are different. It is of interest that the pure multi-beam picture at the centre of the hexagon is about the same intensity regardless of the polarization. This means that in the case of multiple diffraction the polarizations strongly interact and mix.

In the centre of the picture the intensity level is approximately equal to $\exp(-12) = 6 \times 10^{-6}$. Such a strong decrease in the intensity can be explained by the fact that the size of the computational domain is approximately 1.6×10^7 μm^2, which is about 2×10^6 times greater than the area size of the two-dimensional slit, and the size of the image area of the crystal is only a few times smaller. Therefore, the intensity inside the slit is scattered by the crystal inside a huge area. Losses to absorption are also possible, but this leads to the fact that not all of the crystal image areas are illuminated equally. A discussion of the mechanisms of interference fringe formation is beyond the scope of this work.

Fig. 5 shows the section topographs for two polarizations of the incident beam and for the distance of 5 m between the two-dimensional slit and the detector. The axes are the same as in Fig. 4. It should be noted that to obtain this result by the method of direct solution of multi-beam Takagi equations, which was used by Okitsu (2003) and Okitsu *et al.* (2003), is practically impossible, even using a supercomputer. In this paper the result was obtained on a standard laptop computer.

As can be seen from the figure, the distance primarily deforms the two-beam stripes. The two-beam 220 stripes are especially strongly deformed, and these deformations are different in different directions. The central part of the two-beam stripes increases its width inside the polygon, while the thickness of the bridge between the stripes does not change. On the other side of the central part a fragment of the two-beam stripe grows outside of the polygon which corresponds to the angles of pure two-beam diffraction.

Comparing Figs. 3 and 5 it is easy to understand that the right part of the two-beam stripe in Fig. 5 corresponds to the angular region on the right in Fig. 3 and *vice versa*. A rough estimate of the size of the two-beam stripe region can be obtained using the geometrical optics approach. Let us neglect the curvature of the dispersion surface. In this approximation we have a simple correspondence between the coordinate ξ in the topograph, counted from the centre of the two-beam stripe along its direction, and the angle φ in the map of angular dependence (Fig. 3), namely $\xi = z\varphi$, where φ is counted similarly to ξ.

Since the angle between the two-beam stripe and the X axis is small in our case, we can approximately replace ξ by x and φ by θ. The maximum value of the angle θ in Fig. 3 is $\theta_m = 80$ μrad. Therefore $x_m = 0.4$ mm at a distance of 5 m. This estimate corresponds to the length of the fragment outside of the polygon. The other part of the stripe, which is

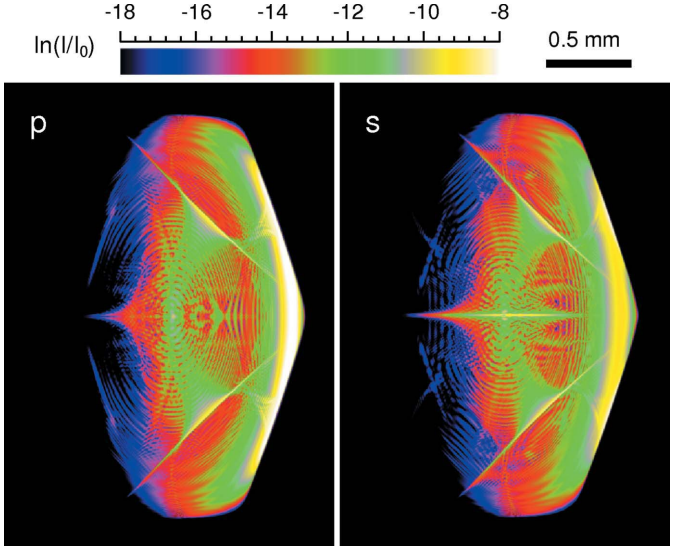

Figure 4
The section topograph of the six-beam diffraction for the distance of 1 cm between the slit and the detector. A logarithm of the transmitted-beam intensity is shown for two polarization states of the incident wave, p (left) and s (right). The horizontal axis corresponds to the x coordinate shown in Fig. 2. Both axes have the same units which are shown above the picture.

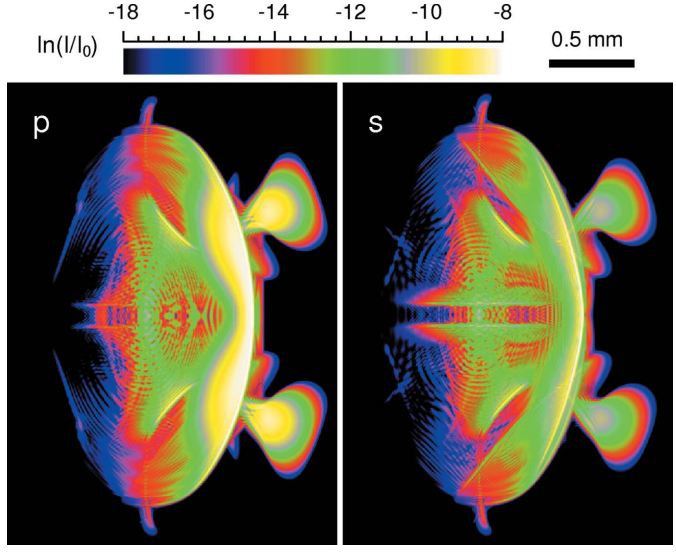

Figure 5
The section topograph of the six-beam diffraction for the distance of 5 m between the slit and the detector. A logarithm of the transmitted-beam intensity is shown for two polarization states of the incident wave, p (left) and s (right). The axes and units are the same as in Fig. 4.

directed inwards, interferes with the six-beam area and looks like a more complicated distribution.

In experiments with a laboratory X-ray source the angular divergence of radiation is very large, so long two-wave stripes are clearly visible even at a distance of 2 m or less. However, the area between them in the form of an arc remains. This arc was first observed by Umeno (1970). Using a synchrotron-radiation source such an experiment is also possible if the two-dimensional slit is replaced by a compound refractive lens (Snigirev *et al.*, 1996). However, the section topograph shows a pure six-beam diffraction area more accurately, so such an experiment is preferable.

As for the weak two-beam stripes, they are entirely located within a six-beam area and interfere with it. The resulting interference leads to the appearance of a band of very weak intensity. It looks like the stripe is cut off and moved apart. This effect is not clear and requires further investigation.

The calculation for the distance of 10 m showed that the above tendencies of the topograph change are enhanced, namely the arc moves closer to the centre, the six-beam area is seen partly outside the arc and partially overlaps by strong two-beam 220 stripes. In general, the picture becomes less expressive and more complex. Since this distance is at the limit of experimental possibilities with a small two-dimensional slit at synchrotron-radiation sources, the corresponding images are not displayed.

Acknowledgements

DRK is grateful to the European programme 'Extreme Light Infrastructure CZ.1.05/1.1.00/02.0061' for financial support.

References

Afanas'ev, A. M. & Kohn, V. G. (1977*a*). *Acta Cryst.* A**33**, 178–184.
Afanas'ev, A. M. & Kon, V. G. (1977*b*). *Fiz. Tverd. Tela (Leningr.)*, **19**, 1775–1783.
Afanas'ev, A. M. & Kon, V. G. (1977*c*). *Sov. Phys. Solid State*, **19**, 1035–1040.
Chang, S.-L. (1982*a*). *Appl. Phys. Lett.* **40**, 793.
Chang, S.-L. (1982*b*). *Z. Naturforsch. Teil A*, **37**, 501–504.
Heyroth, F., Höche, H.-R. & Eisenschmidt, C. (1999). *J. Appl. Cryst.* **32**, 489–496.
Hildebrandt, G., Stephenson, J. D. & Wagenfeld, H. (1975). *Z. Naturforsch. Teil A*, **30**, 697–707.
Huang, T. C., Tillinger, M. H. & Post, B. (1973). *Z. Naturforsch. Teil A*, **28**, 600–603.
Joko, T. & Fukuhara, A. (1967). *J. Phys. Soc. Jpn*, **22**, 597–604.
Kohn, V. G. (1987*a*). *Kristallografia (Moscow)*, **32**, 844–851.
Kohn, V. G. (1987*b*). *Sov. Phys. Crystallogr.* **32**, 496–500.
Kohn, V. G. (2006*a*). *Kristallografia (Moscow)*, **51**, 1001–1005.
Kohn, V. G. (2006*b*). *Crystallogr. Rep.* **51**, 936–940.
Kohn, V. G. & Smirnova, I. A. (2015). *Acta Cryst.* A**71**, 519–525.
Kohn, V., Snigireva, I. & Snigirev, A. (2000). *Phys. Rev. Lett.* **85**, 2745–2748.
Kohn, V., Snigireva, I. & Snigirev, A. (2001). *Opt. Commun.* **198**, 293–309.
Kohn, V. G. & Toneyan, A. H. (1986). *Acta Cryst.* A**42**, 441–449.
Kon, V. G. (1976*a*). *Fiz. Tverd. Tela (Leningr.)*, **18**, 2538–2545.
Kon, V. G. (1976*b*). *Sov. Phys. Solid State*, **18**, 1482–1486.
Kon, V. G. (1977*a*). *Fiz. Tverd. Tela (Leningr.)*, **19**, 3567–3574.
Kon, V. G. (1977*b*). *Sov. Phys. Solid State*, **19**, 2085–2089.
Kshevetskii, S. A. & Mikhailyuk, I. R. (1976*a*). *Kristallografia (Moscow)*, **21**, 381–382.
Kshevetskii, S. A. & Mikhailyuk, I. R. (1976*b*). *Sov. Phys. Crystallogr.* **21**, 209–210.
Okitsu, K. (2003). *Acta Cryst.* A**59**, 235–244.
Okitsu, K., Imai, Y., Ueji, Y. & Yoda, Y. (2003). *Acta Cryst.* A**59**, 311–316.
Okitsu, K., Yoda, Y., Imai, Y. & Ueji, Y. (2011). *Acta Cryst.* A**67**, 550–556.
Okitsu, K., Yoda, Y., Imai, Y., Ueji, Y., Urano, Y. & Zhang, X. (2006). *Acta Cryst.* A**62**, 237–247.
Snigirev, A., Kohn, V., Snigireva, I. & Lengeler, B. (1996). *Nature (London)*, **384**, 49–51.
Takagi, S. (1962). *Acta Cryst.* **15**, 1311–1312.
Umeno, M. (1970). *Phys. Status Solidi (A)*, **2**, K203–K205.
Umeno, M. (1972). *Phys. Status Solidi (A)*, **11**, 501–511.
Umeno, M. (1976*a*). *Phys. Status Solidi (A)*, **37**, 561–570.
Umeno, M. (1976*b*). *Phys. Status Solidi (A)*, **38**, 701–711.